Attenuation of light in different rock types and implications for rock surface luminescence dating

Ou, X. J.; Roberts, H. M.; Duller, G. A. T.; Gunn, M. D.; Perkins, W. T.

Published in:
Radiation Measurements

DOI:
10.1016/j.radmeas.2018.06.027

Publication date:
2018

Citation for published version (APA):
Ou, X. J., Roberts, H. M., Duller, G. A. T., Gunn, M. D., & Perkins, W. T. (2018). Attenuation of light in different rock types and implications for rock surface luminescence dating. *Radiation Measurements*, *120*, 305-311. https://doi.org/10.1016/j.radmeas.2018.06.027

Radiation Measurements 120 (2018) 305–311

Contents lists available at ScienceDirect

Radiation Measurements

journal homepage: www.elsevier.com/locate/radmeas

Attenuation of light in different rock types and implications for rock surface luminescence dating

X.J. Ou[a,c,*], H.M. Roberts[a], G.A.T. Duller[a], M.D. Gunn[b], W.T. Perkins[a]

[a] Department of Geography and Earth Sciences, Aberystwyth University, Ceredigion, SY23 3DB, UK
[b] Department of Physics, Aberystwyth University, Ceredigion, SY23 3BZ, UK
[c] School of Geography and Tourism, Jiaying University, Meizhou, 514015, China

ARTICLE INFO

Keywords:
Rock surface dating
$IRSL_{50}$
Post-IR $IRSL_{225}$
Bleaching
Light attenuation coefficient

ABSTRACT

There is growing interest in rock surface burial and exposure luminescence dating for use in Quaternary science and in archaeology. Such methods have enormous potential both in increasing the range of sedimentary contexts that can be dated, and improving the accuracy and the precision of dating within those contexts. Bleaching of the luminescence signal with depth into the rock surface is likely to vary with lithology. However, previous work on rock surface dating has not systematically studied the differences in light attenuation for rocks of different lithologies, or directly quantified the attenuation of light in different rock surfaces. This study investigates the attenuation of light in different rock types (greywacke, sandstone, two granites and quartzite) using two different approaches: 1) sunlight bleaching experiments, to assess the residual infrared stimulated luminescence signal measured at 50 °C ($IRSL_{50}$) and the post-IR IRSL signal measured at 225 °C (post-IR $IRSL_{225}$) at different depths within the rocks after different durations of exposure to daylight; and, 2) direct measurement of light attenuation in rock slices using a spectrometer. Data from the spectrometer shows that for all rocks, attenuation is greater for shorter wavelengths (~400 nm) than longer ones. A consistent difference in attenuation coefficient is seen when comparing the $IRSL_{50}$ and the post-IR $IRSL_{225}$ signals; this is thought to reflect the different sensitivity of these two signals to infrared and visible light. Direct measurement using a spectrometer is much more rapid than undertaking a bleaching experiment, and also provides wavelength-resolved attenuation data. Comparison of the numerical values from the two approaches is complex, but they yield consistent results. For the samples analysed here, the rocks that appear lightest in colour show the least attenuation of light and the luminescence signals are bleached to the greatest depths, and are thus the most suitable for dating using luminescence.

1. Introduction

Luminescence dating is most commonly applied to 90–300 μm diameter sand-sized or 4–11 μm diameter silt-sized mineral grains extracted from sedimentary deposits (e.g. see review by Rhodes, 2011), where such grain sizes have been produced by natural erosion and weathering of rocks. Resetting of the luminescence signal is achieved by exposure of the sediment grains to daylight during transportation. However, an alternative approach to using sediment grains for dating, is to work with rocks where the mineral grains are still bound together, either by cementation or as a result of the original crystallisation of the rock from a magma, or by subsequent metamorphosis. If the rock is exposed to daylight, the mineral grains exposed at the surface of the rock will have their signal reset in the same way as occurs in sediments, but what makes this method more enticing is that light can also penetrate into the rock, albeit at a much reduced power. Thus if the daylight exposure is sufficiently long, the mineral grains below the rock surface will also have their luminescence signal bleached, and the depth of bleaching into the rock will increase over time.

The potential for dating using rock materials has been studied for many years, especially with regard to its application in dating the construction of buildings using stone blocks (see review by Liritzis, 2011), and also through attempts to directly date stone artefacts (Richards, 1994). In recent years these ideas have been developed further (e.g. Freiesleben et al., 2015; Jenkins et al., 2018; Sohbati et al., 2011, 2015). Two different applications have been developed to exploit measurements of luminescence in rock samples, namely exposure dating and burial dating. Exposure dating can be applied to samples which are currently exposed to daylight, and luminescence measurements are made with increasing depth into the rock, from the outermost light-exposed surface through to a saturated interior; the shape of this bleaching profile with depth into the rock is used to calculate the

* Corresponding author. Department of Geography and Earth Sciences, Aberystwyth University, Ceredigion, SY23 3DB, UK.
E-mail addresses: xio1@aber.ac.uk, ouxianjiao@163.com (X.J. Ou).

https://doi.org/10.1016/j.radmeas.2018.06.027
Received 4 December 2017; Received in revised form 21 June 2018; Accepted 26 June 2018
Available online 28 June 2018

exposure age, i.e. the period of time they have been exposed to daylight (e.g. Sohbati et al., 2012b). In contrast, burial dating looks at rocks which have been exposed to daylight and subsequently buried. The regrowth of the latent luminescence signal in the rock provides a means to date the period of time since burial (e.g. Simms et al., 2011; Sohbati et al., 2012a). In some settings, these two rock-dating methods can be combined to elucidate complex histories of exposure and burial (e.g. Freiesleben et al., 2015).

Rock burial dating is essentially identical in principle to more conventional luminescence dating applied to unconsolidated grains from sedimentary materials, and some studies have effectively treated rocks as large 'grains' and used only the surface of rock clasts for burial dating (e.g. Simms et al., 2011). However, there are significant advantages over sediment dating when the luminescence signal is measured with depth into a buried clast: (1) analysis of the pattern of apparent ages with increasing depth into the rock provides a clear assessment of whether the luminescence signal was bleached prior to deposition, avoiding the need for the complex statistical analysis that is often required for dating sediments (e.g. Duller, 2008; Galbraith and Roberts, 2012; Ou et al., 2015; Smedley et al., 2017); (2) multiple phases of exposure and burial may be revealed (e.g. Freiesleben et al., 2015; Jenkins et al., 2018; Sohbati et al., 2012a); (3) at depths of ~2 mm or greater, a large proportion (> 90% for some samples, Jenkins et al., 2018) of the annual dose originates from the rock itself, reducing the uncertainty in dating due to changes in water content in the surrounding sediment over the period of burial; (4) slices from below the surface are far less susceptible to weathering than sediments or rock surfaces, thereby reducing the likely impact of potential weathering of feldspars, and also avoiding issues such as the loss of surface material through erosion and the potential for post-depositional migration of radionuclides (both of which have implications for the calculation of dose-rate).

To fully exploit these advantages of rock burial dating and avoid simply dating the surface-slice, requires that the OSL signal is bleached before burial to a depth of at least several millimetres into the cobble. While previous studies have recognised that the depth of bleaching into rock depends upon the light transmission of the rock, daylight spectrum, intensity and duration of exposure etc. (e.g. Habermann et al., 2000; Liritzis, 2011; Sohbati et al., 2011, 2015), a systematic study of different rock types to identify the optimal characteristics for luminescence dating has not previously been undertaken. These previous rock luminescence dating studies have mostly focussed on thermoluminescence (TL) dating of carbonates (e.g. Liritzis, 2011; Polikreti, 2007), or looked at a single rock type (e.g. Habermann et al., 2000). Intuitively, and from first principles, rocks that are light in colour, and fine-grained, with a homogeneous mineral composition over the scale of analysis, are anticipated to be better and more uniformly bleached than rocks that are dark in colour, coarse-grained, and have a heterogeneous composition over the scale of analysis. The aim of this study is to investigate light penetration into different rock types, using two independent methods: firstly, a bleaching experiment assessing the attenuation of daylight in rocks by observing the impact upon the magnitude of the luminescence signal arising from trapped charge, and secondly through direct measurement of light attenuation in the rocks. A comparison of these two approaches is presented for rocks of different lithology, selected to include differences in grain size and colour. Finally, the implications of this work for rock surface dating are considered.

2. Samples

Five cobble-sized rocks with a b-axis (intermediate axis) of between 10 and 15 cm, and of different lithologies (Fig. 1), were collected from different sites in the United Kingdom. The sample suite contains sedimentary, igneous, and metamorphic rocks, and hence they vary in grain size, mineral composition and heterogeneity, and colour (see the images of the surfaces and of the cut slices in Fig. 1a and b, respectively). Fig. 1 shows these samples organised primarily by colour; in order from darkest to lightest they are AW-01, CO-01, BTH-01, CW-01 and AP-01. A brief description of each sample follows, whilst further detailed description and images, including from analysis of thin sections, are presented in Supplementary Information. AW-01 is a dark grey, fine grained indurated sedimentary greywacke collected from the Aberystwyth Grits Group at North Beach, Aberystwyth, Wales. CO-01 is a grey medium- to fine-grained sandstone collected from the Pencerrigtewion Member of the Drosgol Formation of late Ordovician age at Carn Owen, Wales. BTH-01 is an orange-coloured, medium-grained, equigranular granite cobble collected from the beach at Borth, Wales, and is likely to have been moved there by glacial processes, hence the origin of the granite is unknown. CW-01 is a pale/cream to pinkish coloured, medium-grained, slightly inequigranular granite cobble collected from Cape Cornwall, approximately 7 km north of Land's End, England, and is likely to be derived from the Land's End granite that outcrops at the site. AP-01 is a pale cream/milky white coloured quartzite, dominated by medium-grained quartz with a quartz cement, collected from the Neoproterozoic Appin Quartzite which is a formation within the Dalradian Supergroup on the north side of Loch Linnhe in Scotland.

3. Daylight bleaching experiment

3.1. Measurements

For the bleaching experiment, the cobbles were cut in half to access the unexposed interior surface. Cutting was undertaken in a room with conventional fluorescent lighting, but exposure of these inner surfaces was kept to a minimum. As is shown later, this exposure had no discernible impact upon the luminescence signal. To explore the impact of exposure to natural daylight, the samples were placed outside on the campus of Aberystwyth University. The experiment was initiated at the end of July 2017. After different periods of exposure (0 day, 1 day, 2 days, 7 days, 14 days, 30 days, 61 days and 91 days), cores ~7 mm in diameter and ~20 mm long were drilled from the fresh surface into the rock, using a bench-mounted pillar drill with a 9 mm external diameter (~7 mm internal diameter) water-cooled sintered diamond core drill bit. These cores were then cut into slices of ~0.4 mm in thickness, using a water-cooled low speed saw mounted with a 0.3 mm thick diamond wafer blade. To ensure that the orientation of each slice was the same, slices were marked with a black permanent pen on the underside. The slices were then cleaned with distilled water in an ultrasonic bath and dried in an oven at a temperature of 50 °C. Finally, all slices were placed in stainless steel cups for luminescence measurement, with their upper side facing up.

Luminescence measurements were carried out on Risø TL/OSL readers (TL-DA-15) with a $^{90}Sr/^{90}Y$ beta irradiation source. The infrared stimulated luminescence (IRSL) signals (870 nm, ~120 mW/cm^{-2}, with 90% optical power) were detected through a combination of a 2 mm Schott BG39 filter and a 2 mm Corning 7–59 blue filter.

A simplified post-IR_{50} $IRSL_{225}$ single aliquot regenerative dose (SAR) protocol (Jenkins et al., 2018), with only two cycles (to measure the natural signal [L_n] and the response to a test dose [T_n], and one regenerative dose signal [L_x] and the corresponding test dose response [T_x]) was used to measure feldspar signals (Table 1). The test dose and the regenerative dose (R_1) were ~20.5 Gy. A low heating rate of 1 °C/s was used for all heating to allow the whole disc to be preheated evenly. At the end of the cycle used to measure the natural (L_n/T_n), an infrared stimulation for 200 s was conducted whilst holding the sample at 280 °C to remove any remaining charge from the measurement cycle and hence to minimize recuperation (Murray and Wintle, 2003). The net IRSL signal was calculated by integrating the first 3.85 s (10 channels) of measurement and subtracting a value derived from the final 19.25 s (50 channels) as background.

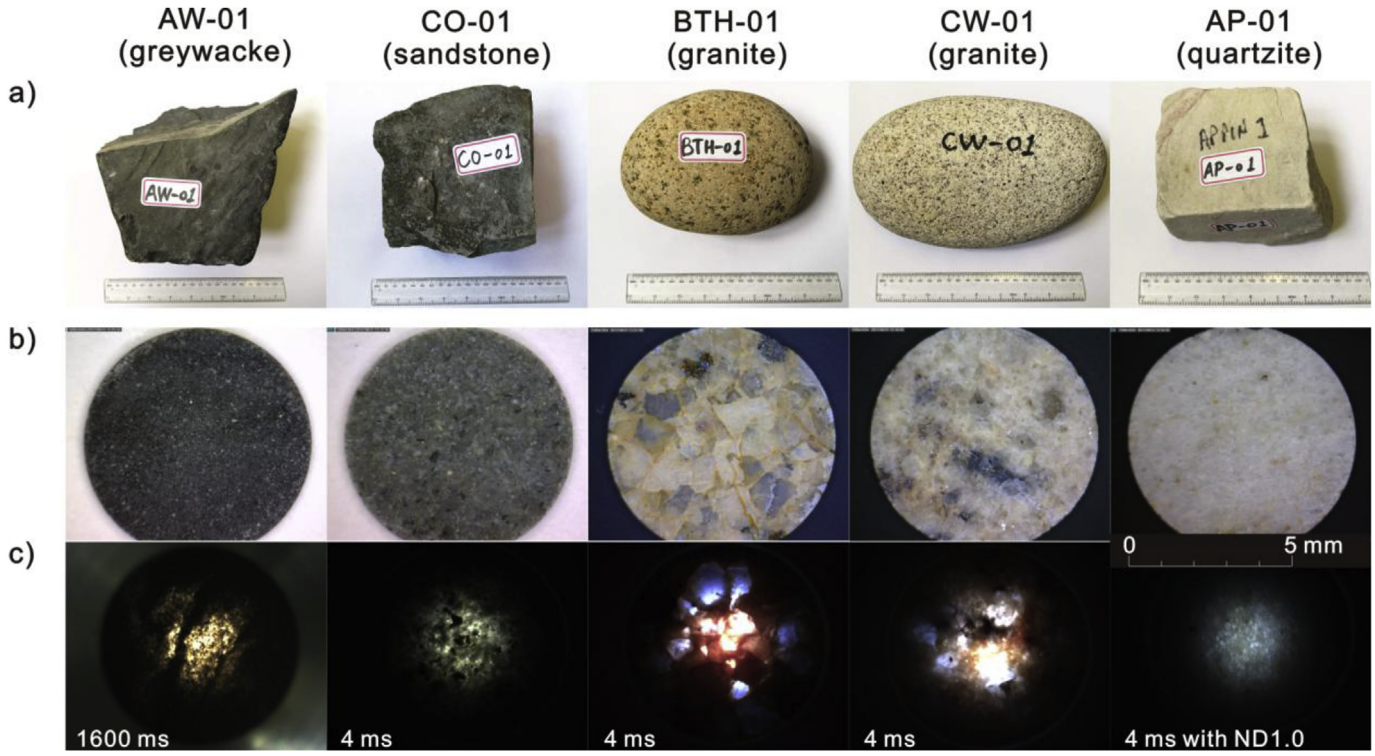

Fig. 1. (A) Photographs of the five original rock samples prior to cutting to expose the saturated interior of each rock for use in the daylight bleaching experiment, (b) their corresponding ~7 mm diameter, ~0.4 mm thick slices prepared from ~20 mm long cores extracted during the daylight bleaching experiment, and (c) transmitted-light CCD images of the slices. From left to right in each panel, a–c: AW-01 (greywacke), CO-01 (sandstone), BTH-01 (granite), CW-01 (granite) and AP-01 (quartzite). The times shown on the transmitted-light images show the integration period used on the camera to obtain sufficient light. Note that for the quartzite slice, an additional ND1.0 filter was added to reduce the brightness.

Table 1
Procedure used for measuring luminescence signal remaining after different periods of daylight exposure (after Jenkins et al., 2018.).

Step	Treatment	Signal
1	No Dose, or Regeneration dose (~20.5 Gy)	
2	Preheat to 250 °C at 1 °C/s and hold for 100 s	
3	IRSL at 50 °C for 200 s	$IRSL_{50}$ L_x
4	IRSL at 225 °C for 200 s	post-IR $IRSL_{225}$ L_x
5	Test dose (~20.5 Gy)	
6	Preheat to 250 °C at 1 °C/s and hold for 100 s	
7	IRSL at 50 °C for 200 s	$IRSL_{50}$ T_x
8	IRSL at 225 °C for 200 s	post-IR $IRSL_{225}$ T_x
9	IRSL at 280 °C for 200 s	

3.2. Results

For each core, the saturation level of the sensitivity-corrected $IRSL_{50}$ or post-IR $IRSL_{225}$ signals (L_n/T_n) under natural irradiation conditions was calculated as the average of the lowermost slices, where there was no sign of the signal having been influenced by daylight exposure. The L_n/T_n ratios for all slices from that core were then normalized to this saturated signal. For sample AP-01, the $IRSL_{50}$ L_n/T_n signal was normalized to the signal averaged from the deepest part of the longest core, as other cores did not reach saturated parts of the sample. The normalized $IRSL_{50}$ and post-IR $IRSL_{225}$ signals were plotted against depth for all five samples (Fig. 2a).

For samples AW-01, CO-01, BTH-01 and CW-01, the $IRSL_{50}$ and post-IR $IRSL_{225}$ data for the cores collected before the experiment started (zero days) are constant through the rock core (Fig. 2a). These samples give a normalized L_n/T_n ratio for zero days exposure of ~1.0 throughout the ~15 mm of sliced rock core. This indicates that no detectable bleaching occurred prior to the start of the experiment, when the rock was initially split into two pieces in white fluorescent light. As the duration of daylight exposure increases from 1 day to 91 days, the effect of daylight exposure can be seen at greater depths. However, the rate at which different rock types bleach as a function of depth varies dramatically (Fig. 2a). Sample AW-01 (greywacke) shows little change in L_n/T_n with exposure time up to 91 days, except in the surface slices. For samples CO-01 (sandstone), BTH-01 (granite) and CW-01 (granite), the effect of bleaching can be seen at ever increasing depth for the $IRSL_{50}$ and post-IR $IRSL_{225}$ signals (Fig. 2a). For the quartzite (AP-01), the post-IR $IRSL_{225}$ signal seems broadly in line with this pattern, but bleaching extends to greater depth than seen for other samples. However, the $IRSL_{50}$ signal does not follow this pattern in the quartzite. For a number of cores no constant value for L_n/T_n is reached at any depth. Only one of the cores appears to reach some saturated level. As demonstrated by the post-IR $IRSL_{225}$ data, sample AP-01 is the sample where the impact of light upon the luminescence signal penetrates the furthest, and it is thought that the $IRSL_{50}$ signal of this sample had been bleached even at depths greater than 15 mm before the start of this experiment.

Another means of comparing the extent to which daylight has bleached the luminescence signal amongst these samples is by plotting the depth into the rock to which the $IRSL_{50}$ and post-IR $IRSL_{225}$ signals have been reduced to 50% of that in saturation (Fig. 2b and c). After 91 days of exposure, the $IRSL_{50}$ signal has reduced by 50% or more at depths down to ~0.2 mm for AW-01, ~1.8 mm for CO-01, ~4 mm for BTH-01 and ~5 mm for CW-01 (Fig. 2b). The depth into quartzite is difficult to determine with the data shown in Fig. 2a, but is estimated to be greater than 10 mm for the $IRSL_{50}$ signal. Similar patterns are seen for the post-IR $IRSL_{225}$ signal (Fig. 2c), but the depth at which the signal has been bleached by 50% is much smaller, as expected given the slower bleaching rate in sediments of this signal compared with that of the $IRSL_{50}$ signal (e.g. Colarossi et al., 2015).

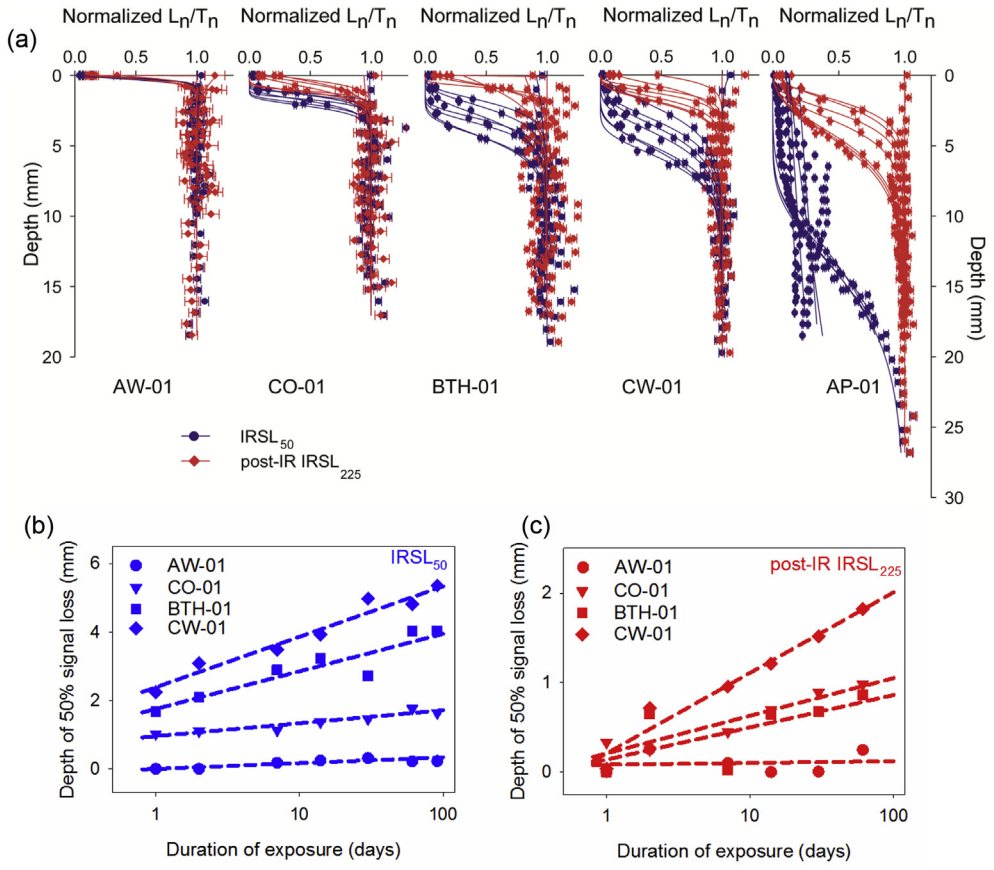

Fig. 2. (A) Changes in normalized L_n/T_n ratios calculated using $IRSL_{50}$ (blue) and post-IR $IRSL_{225}$ (red) signals as a function of depth. Data for five different rock samples are shown after exposure to daylight for periods up to 91 days. With the exception of AP-01, the depth into each rock to which the luminescence signal has been reduced to half its initial signal is also shown for (b) the $IRSL_{50}$ signal and (c) the post-IR $IRSL_{225}$ signal as a function of the duration of exposure to daylight. (For interpretation of the references to colour in this figure legend, the reader is referred to the Web version of this article.)

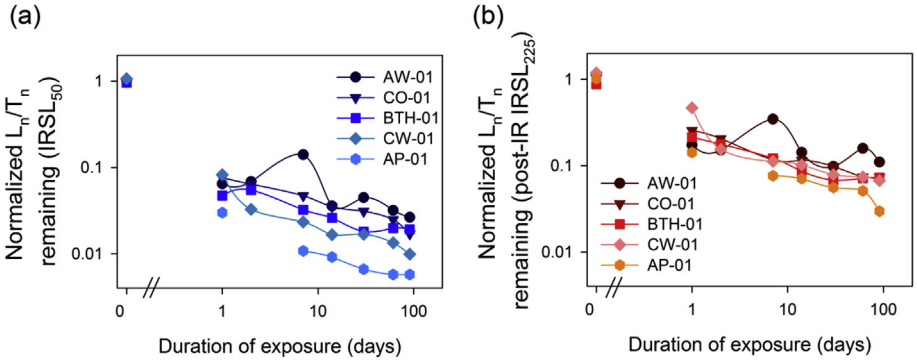

Fig. 3. Remaining luminescence signal (normalized (a) $IRSL_{50}$ and (b) post-IR $IRSL_{225}$ L_n/T_n ratios) in the surface slices of the five different rock types after different durations of exposure.

Fig. 3 shows the normalized $IRSL_{50}$ and post-IR $IRSL_{225}$ signal remaining, derived from the surface slice of each core after different exposure times. As in Fig. 2, the lighter the rock colour, the lower the luminescence signal remaining. The pattern of reduction in signal, and the difference between the $IRSL_{50}$ and post-IR $IRSL_{225}$ signals, is very similar to the observations of Colarossi et al. (2015) who examined separated potassium-rich feldspar grains and used a SOL2 solar simulator for bleaching. However, while it took the 180 μm diameter feldspar grains in the experiment by Colarossi et al. (2015) 2–3 days of continuous exposure to the SOL2 to reach 1% of their initial signal, the surface slice of CW-01 (one of the most rapidly bleaching samples in this study) took 91 days of exposure to natural daylight to reach this same level. The absolute difference in remaining signal between rock types becomes smaller as exposure time increases and the luminescence signals approach zero. After 91 days of exposure, the proportion of the $IRSL_{50}$ signal remaining is low for all samples, being 0.026 ± 0.002 (AW-01), 0.017 ± 0.001 (CO-01), 0.019 ± 0.000 (BTH-01), 0.010 ± 0.000 (CW-01) and 0.006 ± 0.000 (AP-01), respectively (Fig. 3a). The post-IR $IRSL_{225}$ signal shows a similar pattern to that of the $IRSL_{50}$ signal, but with higher levels of signal remaining. After 91 days of exposure, the proportion of the post-IR $IRSL_{225}$ signal remaining is 0.110 ± 0.020 (AW-01), 0.074 ± 0.008 (CO-01), 0.073 ± 0.002 (BTH-01), 0.067 ± 0.002 (CW-01), and 0.030 ± 0.001 (AP-01), respectively (Fig. 3b).

4. Direct measurement of light attenuation

4.1. Measurements

Spectral attenuation coefficient measurements were made on 7 mm diameter rock slices, to assess the reduction in radiant power as light passed through the samples. The attenuation coefficient is a measure of

the combined influence of absorption and scattering per unit length. Samples were mounted at the focussed output of a 150 W Xenon arc lamp. Transmitted light was collected with a Thorlabs CCSA2 cosine corrector to remove directional effects and provide a well-defined 4 mm diameter measurement area. Collected light was coupled via a 400 μm diameter optical fibre to an Ocean Optics Flame spectrometer with a measurement range of 340–1018 nm. The thickness of each sample was measured with an SPI digital micrometer.

The spectral reflectance of each rock type was measured in a separate experiment with an Ocean Optics ISP- REF integrating sphere, fibre-coupled to the Ocean Optics Flame spectrometer. The reflectance was measured in total hemispherical/directional geometry – the sample was illuminated over the full hemisphere and the light reflected in a single direction, ~8° from normal incidence, was measured. Spectral reflectance measurements for rock slices of each lithology were made relative to a Spectralon reflectance standard. For the lighter coloured samples (AP-01, CW-01 and BTH-01), reflection losses of up to 30% at the first surface were observed. For the darker samples (CO-01 and AW-01), the reflectance was negligible as would be expected.

After the lamp had been allowed to warm up and stabilise, a reference measurement was made with no sample in the beam and an exposure time of 2 ms. A total of 15,000 readings were taken to average out fluctuations in the lamp output and give a total measurement time of 30 s. Subsequently, each sample was mounted in the beam and the integration time was adjusted in the software so that the maximum signal reached approximately 90% of the spectrometer's dynamic range. The number of average measurements was adjusted so that the total measurement time was maintained at ~30 s. A dark measurement, taken with the beam blocked, was subtracted from each measurement. The spectral attenuation coefficient (μ) at each wavelength was calculated from the measurements using the Beer-Lambert law corrected for sample reflectance as shown in Eq (1), where ϕ_S and ϕ_R are the spectral flux detected, t_S and t_R are the exposure times for the Sample and Reference measurements respectively, l is the thickness of the sample and R_S is the spectral reflectance of the sample (expressed as the fraction of the incident power that is reflected).

$$\mu = \frac{-Ln\left(\frac{\phi_S}{\phi_R} * \frac{t_R}{t_S} * \frac{1}{1-R_S}\right)}{l} \quad (1)$$

4.2. Results

Slices of varying thickness, from ~0.4 to 2.4 mm, were measured in order to assess whether attenuation changes for thicker slices, e.g. as a result of internal scattering. Fig. 4a shows the results for measurements of attenuation that have not been corrected for thickness l, and these increase linearly with slice thickness (Fig. 4a). This implies that, for these samples, the direct measurements of transmission made on thin slices can be extrapolated to help understand attenuation through the greater thicknesses of rock typically studied for dating, and that internal scattering is not a confounding process.

Fig. 4b shows the attenuation coefficient calculated for each rock type as a function of wavelength, and demonstrates that all rock types have a higher attenuation coefficient at shorter wavelengths, consistent with exobiology studies on a variety of different types of rock (e.g. Smith et al., 2014). This implies that the spectrum to which minerals are exposed will become increasingly biased towards the red and infrared at increasing depth into the rock. The attenuation coefficient of the different rock types varies by up to a factor of 26 times (equivalent to 8 orders of magnitude difference in transmission, Fig. 4b), consistent with the large variation seen in the depth of bleaching observed in Fig. 2.

The datasets shown in Fig. 4 are the attenuation coefficient averaged over the 4 mm diameter area of the centre of each slice, but some samples appear more visually homogeneous than others (Fig. 1). To

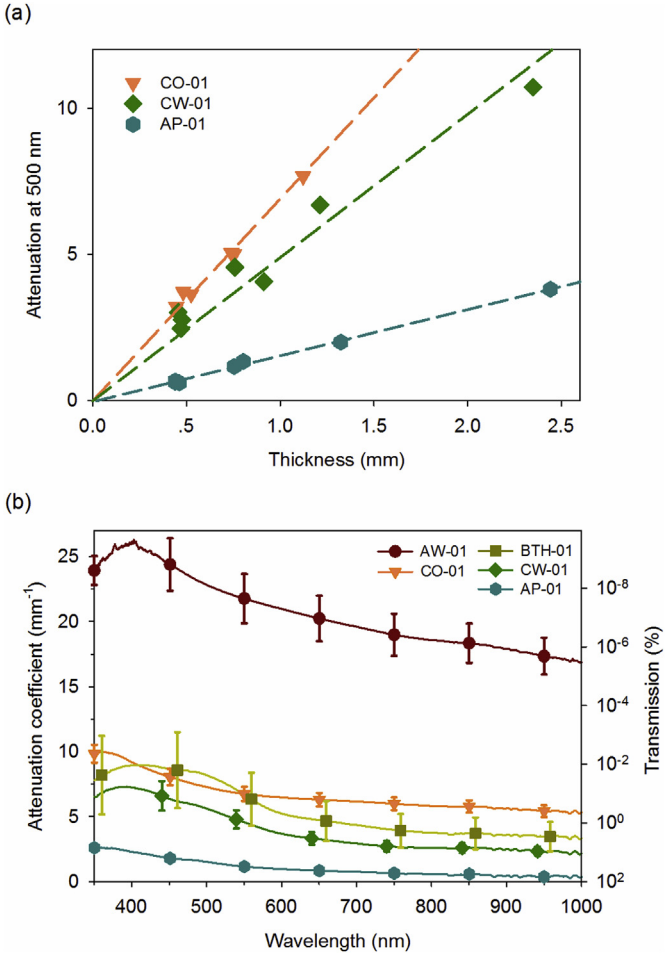

Fig. 4. (A) Attenuation measured at 500 nm for slices of different rock types, varying in thickness from ~0.4 mm to 2.4 mm. Note that for this figure, measurements of attenuation have not been corrected for variations in thickness l as shown in Eq. (1). Data for AW-01 are not shown as it was not possible to measure slices thicker than ~0.4 mm because the attenuation was so great (see Fig. 4b). Data from sample BTH-01 were very scattered, and has not been plotted for clarity. (b) Attenuation coefficient per millimetre as a function of wavelength for each of the five samples. Data from five slices of each sample were averaged, and the standard deviation in these replicates is indicated by the error bars. A correction for reflectance at the surface of the rock slices has been included. Data were collected at a spectral resolution of ~0.4 nm, but symbols and error bars are shown every 100 nm for clarity. For those more familiar with values expressed as transmission, the y-axis on the right hand side is shown.

investigate this, we replaced the spectrometer with a high sensitivity CCD camera and used this to image the light transmitted through each rock type. The integration time needed to obtain sufficient photons to yield a clear image varied with the attenuation coefficient of the samples (Fig. 1c). The relatively small sized (compared to the size of the slice) mineral grains making up the three sedimentary and metamorphic rocks, AW01, CO-01 and AP-01, can be seen distributed throughout the rock slices (Fig. 1b, and Figs. S1–S5), producing a relatively homogeneous pattern of transmission (Fig. 1c). In AW-01 two dark bands can be seen (Fig. 1c), and these are thought to be finer grained sediments, consistent with their deposition as turbidites. Sample CO-01 contains some darker minerals (that can be seen in the optical image Fig. 1b). The two granite samples show large variations in the transmission of light between the different minerals present (primarily quartz, feldspar and biotite), with light preferentially passing through quartz grains and the lighter coloured feldspar. On a fine scale this is likely to cause variability in light exposure of different grains at a similar depth (cf. Meyer et al., these proceedings), though even over the

scale of the images seen in Fig. 1c, such variations may be averaged out. These images are a useful tool for giving us an understanding of how light is passing through the rock and the mineral grains.

5. Discussion

The two independent experiments discussed in sections 3 and 4 clearly show that the attenuation coefficient varies significantly between the five different rocks studied here, and both sets of measurements indicate that for this suite of samples the lightest coloured rocks are those that have the lowest attenuation coefficient of light. The wavelength resolved measurements (Fig. 4b) show that attenuation coefficient varies by as much as a factor of 26 times (8 orders of magnitude change in transmission) between the different rocks (AP-01 has the lowest values and AW-01 the highest). These results highlight the critical role that rock type will make when applying luminescence dating methods to cobble-sized clasts.

To enable comparison of the two experimental approaches, data in Fig. 2a were fitted with the equation described by Sohbati et al. (2011) for the impact of light upon the luminescence signal (L) as a function of depth (x) (Eq (2)). The effect is dependent upon time of exposure (t), light intensity (φ), the photoionization cross section (σ) of the trap responsible for the luminescence signal, and the attenuation coefficient of the light by the rock (μ, mm^{-1}).

$$L(x) = e^{-t\overline{\sigma\varphi_0}(e^{-\mu x})} \quad (2)$$

The average value of μ, the attenuation coefficient of light by the rock (in units of mm^{-1}) is shown for each rock type in Table 2, calculated using both the $IRSL_{50}$ and post-IR $IRSL_{225}$ signals. For CW-01, values of μ were obtained for all exposure times, but for the other samples, where attenuation was greater, values of μ for short periods of daylight exposure, especially for some of the post-IR $IRSL_{225}$ data, could not be accurately determined because there were insufficient data points to allow fitting of Eq. (2). Where values of μ could be calculated for the post-IR $IRSL_{225}$ data they tend to be more scattered than the data for the $IRSL_{50}$ signal because of the limited number of slices where signal loss is seen (Fig. 2a). The values of μ obtained from the $IRSL_{50}$ signal for the two granites are 0.74 ± 0.04 mm^{-1} for CW-01 and 1.17 ± 0.21 mm^{-1} for BTH-01. They are close to those previously reported for granite samples (e.g. 0.8 ± 0.2 (099901) and 0.51 ± 0.19 mm^{-1} (099902) from Sohbati et al. (2011), and 0.61 ± 0.14 mm^{-1} from Sohbati et al. (2015)).

The attenuation coefficients calculated for the post-IR $IRSL_{225}$ signals from Fig. 2a are typically larger than those from the $IRSL_{50}$ signal (Table 2). Since the two luminescence signals were obtained from the same rock slices, this cannot be explained by small scale variations in the rocks. One explanation for this difference is suggested by the measurements described in Section 4.2 showing variations in the attenuation coefficient as a function of wavelength. Fig. 4b shows that all of the rocks exhibited larger attenuation coefficients for shorter wavelengths than those in the near infrared, and perhaps the difference in attenuation coefficients between the $IRSL_{50}$ and post-IR $IRSL_{225}$ signals reflects variations in the efficiency with which light at different wavelengths is able to remove charge from the defects being probed.

Table 2
Values of attenuation coefficient (in mm^{-1}) measured in the five rocks, based on fitting the $IRSL_{50}$ and post-IR $IRSL_{225}$ bleaching data (Fig. 2) and on direct measurements using a Xenon arc lamp (Fig. 4). Data for direct measurements are given for two wavelengths, 500 nm and 860 nm, as explained in the text.

Sample	Attenuation coefficient from daylight bleaching (mm^{-1})		Attenuation coefficient from direct measurement (mm^{-1})	
	$IRSL_{50}$	post-IR $IRSL_{225}$	500 nm	860 nm
AW-01	6.43 ± 1.10	–	22.8 ± 1.97	18.3 ± 1.50
CO-01	3.06 ± 0.50	2.86 ± 0.60	7.28 ± 0.58	5.77 ± 0.47
BTH-01	1.17 ± 0.21	2.67 ± 1.33	8.20 ± 2.68	3.72 ± 1.22
CW-01	0.74 ± 0.04	1.86 ± 0.47	5.62 ± 0.83	2.61 ± 0.39
AP-01	0.24 ± 0.02	0.68 ± 0.23	1.52 ± 0.10	0.55 ± 0.18

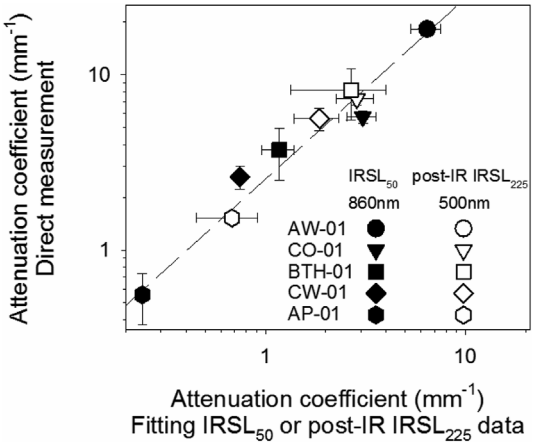

Fig. 5. A comparison of results obtained using two methods for estimating the attenuation coefficient of the five rock samples. Data on the x-axis were obtained by fitting either the $IRSL_{50}$ or the post-IR $IRSL_{225}$ bleaching data in Fig. 2a, while the data on the y-axis were obtained using the direct measurement of light to calculate the attenuation coefficient (Fig. 4b) at 500 and 860 nm.

Fig. 5 compares attenuation coefficients obtained from direct measurements with those obtained from fitting the $IRSL_{50}$ and post-IR $IRSL_{225}$ data from Fig. 2a. Spooner (1994) measured the bleaching energy required at various wavelengths to reduce the IRSL signal measured at room temperature (similar to the $IRSL_{50}$ signal in this study) from a microcline feldspar by 10, 50 or 90%. He showed that from 400 to 740 nm, there was an exponential rise in the energy (J/m^2) required to reduce the IRSL signal but, as was already known (Hütt et al., 1988), there is a resonance in the excitation spectrum for feldspars centred at ~860 nm (Barnett and Bailiff, 1997), and hence in Fig. 5 the attenuation coefficient from Fig. 4b at 860 nm is plotted against the $IRSL_{50}$ derived value. Wavelength-resolved bleaching experiments such as those undertaken by Spooner (1994) have not been undertaken for the post-IR $IRSL_{225}$ signal. However, based on the feldspar models of Jain and Ankjaergaard (2011) and Jain et al. (2015), one would anticipate that after removal of charge from traps which are sensitive to infrared by the $IRSL_{50}$ measurement, the post-IR IRSL measurement will sample charge from defects that can only be emptied by higher energy photons (e.g. in the green and blue). The solar spectrum at ground level peaks between 500 and 600 nm, and when coupled with the stimulation spectrum of feldspars, the shorter wavelengths are likely to have the most impact upon the post-IR IRSL signal. Thus in Fig. 5, the attenuation coefficient at 500 nm (from Fig. 4b) is plotted against the post-IR $IRSL_{225}$ derived value (from Fig. 2a). The values of attenuation derived from direct measurement are consistently larger than those derived from bleaching experiments (Fig. 5). Direct comparison between the values obtained from the two methods is complex, since the response of the luminescence signal integrates the impact of light at various wavelengths and depends upon the photo-ionisation cross-section of the defect being probed. However, the ranked order of the samples is identical across the two methods used to examine light attenuation (Fig. 5), suggesting that the daylight bleaching experiment (Fig. 2) and the direct attenuation measurements (section 4.2; Fig. 4b) give rise to comparable datasets.

6. Conclusions

In this study, two independent methods for assessing the

attenuation of light through five different rock types were examined, using a daylight bleaching experiment over a duration of 91 days and comparing this against direct measurement of light attenuation in the laboratory. The IRSL signals bleached to different depths within the various rock types during the daylight bleaching experiment, and as observed in previous studies of unconsolidated sediments, the $IRSL_{50}$ signal bleached at a faster rate than the post-IR $IRSL_{225}$ signal. The IRSL signals for the lighter-coloured rock samples were bleached to the greatest depths. For example, after 91 days of daylight bleaching, the $IRSL_{50}$ signal was bleached to half of its initial intensity at a depth of 0.2 mm for the dark grey fine-grained greywacke sample, ~1.8 mm for the grey medium-to fine-grained sandstone, and ~4 and ~5 mm for the two granite samples, and in excess of 10 mm for the cream/milky white quartzite sample. Direct measurements of the attenuation of light also varied dramatically for the different rock types, with the attenuation coefficient varying by up to a factor of 26 times (equivalent to 8 orders of magnitude difference in transmission) between rock types.

Direct measurements using the spectrometer also demonstrated a strong wavelength dependence of the attenuation coefficients (Fig. 4b). A striking result from the daylight bleaching experiment is that the $IRSL_{50}$ and post-IR $IRSL_{225}$ signals give different attenuation coefficients (Table 2), and this is thought to be due to differences in the sensitivity of the two signals to different wavelengths of light. It would appear that the post-IR $IRSL_{225}$ signal suffers both from a slower rate of bleaching (Colarossi et al., 2015) and also a larger attenuation coefficient, making its use in luminescence surface dating more difficult than the $IRSL_{50}$ signal.

Although the two different ways of assessing the attenuation of light in different rock types gave data that were effectively in agreement with each other, direct measurement of attenuation offers some advantages over daylight bleaching experiments, by revealing the spatial variability in attenuation within each sample, and between rock types. Additionally, direct measurement of attenuation is more rapid than daylight bleaching, allows for easier quantification of measurement uncertainties and examination of replicate analyses and, perhaps most significantly, can give wavelength-resolved data. Daylight bleaching experiments will continue to be valuable since they provide a direct measure of the loss of luminescence, integrating the effects of different wavelengths within the solar spectrum upon the various luminescence signals that are measured.

Finally, the comparison of the dramatically different bleaching depths observed for different rock types in this study has implications for the selection and preparation of materials for burial dating of rocks. One of the major strengths of burial dating of rocks is that if a clast has been exposed to sufficient sunlight, then it will give the same finite value of age throughout the upper portions of the clast, thereby offering the chance to screen the rock age data and hence avoiding the need for the application of complex statistical models to analyse potentially incompletely bleached D_e distributions. However, to maximise the chance of working with well-bleached clasts, attention should be paid to identifying in the field those rock-types that are likely to be the most susceptible to bleaching of the luminescence signal. Additionally, slicing the clasts as finely as possible (~0.4 mm thickness with a 300 μm thick blade in this study), or potentially obtaining spatially-resolved D_e data from a continuous rock slice which extends from the outer-most to inner-most parts of the clast will improve the potential to identify well-bleached clasts by maximising the number of potential replicate D_e determinations that can be obtained with depth.

Acknowledgements

This project has received funding from the European Union's Horizon 2020 research and innovation programme under the Marie Skłodowska-Curie grant agreement No 663830. XJO also thanks support from the National Natural Sciences Foundation of China (grants 41371080), and Tommy Ridgway, Geraint Jenkins, and Hollie Wynne for help in the laboratory. Research in Next Generation Luminescence methods in Aberystwyth is supported by NERC grant CC003, and by HEFCW infrastructure funding for SPARCL. This work was also supported by the UK Space Agency CREST3 program under grant ST/P001998/1. The comments of Mayank Jain and an anonymous referee are gratefully acknowledged.

Appendix A. Supplementary data

Supplementary data related to this article can be found at http://dx.doi.org/10.1016/j.radmeas.2018.06.027.

References

Barnett, S.M., Bailiff, I.K., 1997. Infrared stimulation spectra of sediments containing feldspars. Radiat. Meas. 27, 237–242.
Colarossi, D., Duller, G.A.T., Roberts, H.M., Tooth, S., Lyons, R., 2015. Comparison of paired quartz OSL and feldspar post-IR IRSL dose distributions in poorly bleached fluvial sediments from South Africa. Quat. Geochronol. 30, 233–238.
Duller, G.A.T., 2008. Single-grain optical dating of Quaternary sediments: why aliquot size matters in luminescence dating. Boreas 37, 589–612.
Freiesleben, T., Sohbati, R., Murray, A., Jain, M., Khasawneh, S.A., Hvidt, S., Bo, J., 2015. Mathematical model quantifies multiple daylight exposure and burial events for rock surfaces using luminescence dating. Radiat. Meas. 81, 16–22.
Galbraith, R.F., Roberts, R.G., 2012. Statistical aspects of equivalent dose and error calculation and display in OSL dating: an overview and some recommendations. Quat. Geochronol. 11, 1–27.
Habermann, J., Schilles, T., Kalchgruber, R., Wagner, G.A., 2000. Steps towards surface dating using luminescence. Radiat. Meas. 32, 847–851.
Hütt, G., Jaek, I., Tchonka, J., 1988. Optical dating: K-feldspars optical response stimulation spectra. Quat. Sci. Rev. 7, 381–385.
Jain, M., Ankjaergaard, C., 2011. Towards a non-fading signal in feldspar: insight into charge transport and tunnelling from time-resolved optically stimulated luminescence. Radiat. Meas. 46, 292–309.
Jain, M., Sohbati, R., Guralnik, B., Murray, A.S., Kook, M., Lapp, T., Prasad, A.K., Thomsen, K.J., Buylaert, J.P., 2015. Kinetics of infrared stimulated luminescence from feldspars. Radiat. Meas. 81, 242–250.
Jenkins, G.T.H., Duller, G.A.T., Roberts, H.M., Chiverrell, R.C., Glasser, N.F., 2018. A new approach for luminescence dating glaciofluvial deposits - high precision optical dating of cobbles. Quat. Sci. Rev. 192, 263–273.
Liritzis, I., 2011. Surface dating by luminescence: an overview. Geochronometria 38, 292–302.
Murray, A.S., Wintle, A.G., 2003. The single aliquot regenerative dose protocol: potential for improvements in reliability. Radiat. Meas. 37, 377–381.
Meyer, M.C., Gliganic, L.A., Jain, M., Sohbati, R., Schmidmair, D., These proceedings. Lithological controls on light penetration into rock surfaces – implications for OSL and IRSL surface exposure dating. Radiat. Meas.. doi:10.1016/j.radmeas.2018.03.004.
Ou, X.J., Duller, G.A.T., Roberts, H.M., Zhou, S.Z., Lai, Z.P., Chen, R., Chen, R.R., Zeng, L.H., 2015. Single grain optically stimulated luminescence dating of glacial sediments from the Baiyu valley, southeastern Tibet. Quat. Geochronol. 30, 314–319.
Polikreti, K., 2007. Detection of ancient marble forgery: techniques and limitations. Archaeometry 49, 603–619.
Rhodes, E.J., 2011. Optically stimulated luminescence dating of sediments over the past 200,000 years. Annu. Rev. Earth Planet Sci. 39, 461–488.
Richards, M., 1994. Luminescence Dating of Quartzite from the Diring Yuriakh Site. Unpublished MSc thesis. Simon Fraser University, Canada.
Simms, A.R., DeWitt, R., Kouremenos, P., Drewry, A.M., 2011. A new approach to reconstructing sea levels in Antarctica using optically stimulated luminescence of cobble surfaces. Quat. Geochronol. 6, 50–60.
Smedley, R.K., Scourse, J.D., Small, D., Hiemstra, J.F., Duller, G.A.T., Bateman, M.D., Burke, M.J., Chiverrell, R.C., Clark, C.D., Davies, S.M., 2017. New age constraints for the limit of the British–Irish ice sheet on the isles of scilly. J. Quat. Sci. 32, 48–62.
Smith, H.D., Baqué, M., Duncan, A.G., Lloyd, C.R., McKay, C.P., Billi, D., 2014. Comparative analysis of cyanobacteria inhabiting rocks with different light transmittance in the Mojave Desert: a Mars terrestrial analogue. Int. J. Astrobiol. 13, 271–277.
Sohbati, R., Murray, A.S., Buylaert, J.P., Almeida, N.A.C., Cunha, P.P., 2012a. Optically stimulated luminescence (OSL) dating of quartzite cobbles from the Tapada do Montinho archaeological site (east-central Portugal). Boreas 41, 452–462.
Sohbati, R., Murray, A.S., Chapot, M.S., Jain, M., Pederson, J., 2012b. Optically stimulated luminescence (OSL) as a chronometer for surface exposure dating. J. Geophys. Res. Sol. Ea 117.
Sohbati, R., Murray, A.S., Jain, M., Buylaert, J.P., Thomsen, K.J., 2011. Investigating the resetting of OSL signals in rock surfaces. Geochronometria 38, 249–258.
Sohbati, R., Murray, A.S., Porat, N., Jain, M., Avner, U., 2015. Age of a prehistoric "Rodedian" cult site constrained by sediment and rock surface luminescence dating techniques. Quat. Geochronol. 30, 90–99.
Spooner, N.A., 1994. The anomalous fading of infrared-stimulated luminescence from feldspars. Radiat. Meas. 23, 625–632.